Single-particle strength from nucleon transfer in oxygen isotopes: Sensitivity to model parameters

F. Flavigny,[1] N. Keeley,[2] A. Gillibert,[3] and A. Obertelli[3,4]
[1]*Institut de Physique Nucléaire, CNRS-IN2P3, Université Paris-Sud, Université Paris-Saclay, 91406 Orsay, France*
[2]*National Centre for Nuclear Research, ul. Sołtana 7, PL-05400 Otwock, Poland*
[3]*IRFU, CEA, Université Paris-Saclay, F-91191 Gif-sur-Yvette, France*
[4]*Institut für Kernphysik, Technische Universität Darmstadt, 64289 Darmstadt, Germany*

(Received 12 October 2017; published 1 March 2018)

In the analysis of transfer reaction data to extract nuclear structure information the choice of input parameters to the reaction model such as distorting potentials and overlap functions has a significant impact. In this paper we consider a set of data for the (d,t) and $(d,{}^3\mathrm{He})$ reactions on ${}^{14,16,18}\mathrm{O}$ as a well-delimited subject for a study of the sensitivity of such analyses to different choices of distorting potentials and overlap functions with particular reference to a previous investigation of the variation of valence nucleon correlations as a function of the difference in nucleon separation energy $\Delta S = |S_p - S_n|$ [Phys. Rev. Lett. **110**, 122503 (2013)].

DOI: 10.1103/PhysRevC.97.034601

I. INTRODUCTION

Direct nuclear reactions have been one of the key techniques for the investigation of nuclear structure since their first development [1–5] due to their sensitivity to the overlap between the initial- and final-state wave functions. For example, single-nucleon transfer reactions were shown to favor the population of states in the final nucleus, which could be described as single-particle excitations with respect to its ground-state configuration. The main assumption made in most current interpretations of direct reactions is that the measured cross section σ can be factorized into a single-particle reaction cross section σ_{sp} and a so-called spectroscopic factor (SF). The SF contains part of the dependence on the structure of the initial and final states since it is defined as the norm of the overlap function between these states. On the other hand σ_{sp} is related to the dynamics of the reaction and contains all the dependence on incident energy and angle but still includes a strong dependence on the radial shape of the overlap functions involved. Experimentally, the SFs are obtained by normalizing the calculated cross section (σ_{sp}) to the measured cross section and as such are intrinsically model dependent. In use now for almost sixty years, this method of extracting SFs contributed to forge our current understanding of shell structure and its evolution away from stability [6–10].

Ideally, measured cross sections should be interpreted directly by comparison with theoretical predictions obtained by solving the full many-body time-dependent Schrödinger equation, treating consistently nuclear structure and reaction dynamics. While progress has been made in this direction [11–13], it remains computationally very demanding and limited in its range of application and is thus not yet usable for systematic studies. The problem of reaction model dependence and consistency arises inevitably when one attempts to compare results from different energy regimes or probes, as addressed in some cases using stable nuclei [14,15], but it can also appear within a given reaction framework if input parameters are different.

For single-nucleon transfer reactions at low energies several formalisms are available [16] from the zero-range distorted-wave Born approximation (DWBA) through finite-range coupled reaction channels (CRCs). The first choice to be made in any analysis is therefore that of an appropriate reaction model. In making this choice the approximations inherent in these formalisms should be carefully borne in mind; for example, the DWBA is predicated upon the assumption that the elastic scattering is the dominant process and if this is not the case its use can lead to spurious results or it may not be able to give an adequate description of the shape of the reaction angular distributions, making the extraction of SFs even more problematical. However, in some cases the situation is not as simple, since two calculations based on different approximations can lead to a similar degree of agreement with the shape of the experimental angular distribution but manifest significant differences in their absolute value and thus lead to very different SFs.

The second choice known strongly to impact the calculated cross sections is that of the optical potentials necessary to solve the scattering problem. While the entrance channel potential can always be constrained, at least in principle, from a simultaneous measurement of the elastic scattering with the transfer reaction of interest, the exit channel poses a different problem. Either a separate dedicated elastic scattering measurement must be made—not always possible since, especially with the use of exotic beams, one or other of the exit channel nuclei may be unbound—or global optical potentials fitted to data over a limited range of projectile energy and target mass must be employed. This is a particular problem for systems involving ${}^3\mathrm{He}$ or ${}^3\mathrm{H}$ ejectiles since only a few global potentials are available for these nuclei and particular choices can lead to significant differences in the extracted SFs. Also, even when appropriate elastic scattering data are available it is well known that different potentials giving equivalent fits to these data can lead to quite different results for the transfer cross sections, see, e.g., Ref. [17] for a recent investigation of how these uncertainties may be quantified.

 ©2018 American Physical Society

Finally, the choice of the overlap functions (OFs) involved in the extraction of the SFs is crucial since it can considerably alter the magnitude of the calculated angular distributions although it normally does not modify significantly their shape. The OFs are usually calculated using the so-called well-depth prescription where the transferred nucleon (or cluster) is bound in a Woods-Saxon well of fixed geometry with a depth adjusted to yield the experimental binding energy. The choice of the geometry of the well, particularly the radius, will impact the value of the extracted SF. The use of a Woods-Saxon well of radius $1.25 \times A^{1/3}$ fm and diffuseness $a = 0.65$ fm remains widespread even if this convention, deriving as it does from the real central potential of a global optical model parametrization adopted in the 1960s to fit nucleon-nucleus elastic scattering data [18–20], has no particular physical justification in this context.

In this paper we attempt to quantify these three kinds of uncertainty, namely, the reaction framework, optical potentials, and overlap functions, for the (d,t)[1] and $(d,{}^3\mathrm{He})$ single-nucleon pickup reactions in the spirit of other recent theoretical studies mainly focused on (d,p) stripping reactions [17,21]. The data set from our previous study of these reactions on the oxygen isotopes [31] forms a well-delimited subject for the purpose of illustrating these model dependencies in a quantitative way, although we do not attempt a statistically rigorous assessment of the uncertainties as was done recently for optical model parameters [17]. As a conclusion of this study, we address the importance of these model dependencies for the interpretation of valence-nucleon correlations as a function of the difference in separation energy $\Delta S = |S_p - S_n|$, a subject well discussed in the literature (see Refs. [22–31] and references therein).

II. EXPERIMENTAL DATA SETS

The $^{14}\mathrm{O}(d,d)^{14}\mathrm{O}$ elastic scattering, $^{14}\mathrm{O}(d,t)^{13}\mathrm{O}$ single neutron stripping and $^{14}\mathrm{O}(d,{}^3\mathrm{He})^{13}\mathrm{N}$ single proton stripping reactions were measured in a dedicated experiment, described briefly in Ref. [31]. We recapitulate the description of the experimental setup and give more details here. A $^{14}\mathrm{O}^{8+}$ beam was accelerated to 18.1 MeV/nucleon at the SPIRAL facility (GANIL, France) with a mean intensity of 6×10^4 pps. The purity of the beam, always higher than 85%, was controlled with a time-of-flight measurement before the target leading to an unambiguous particle identification, event by event, necessary to reject the $^{14}\mathrm{N}^{7+}$ contaminant. A global validation of the setup was performed with the stable beam ^{14}N at 18 MeV/nucleon. Deuterated polypropylene CD_2 targets were used (where D denotes deuterium, ^{2}H): 0.5 mg/cm^2 thick for the $(d,{}^3\mathrm{He})$ channel, 1.5 mg/cm^2 thick for the elastic scattering and 8.5 mg/cm^2 thick for the (d,t) channel. These choices result from a compromise between counting rate and the energy of the recoil nuclei, much larger for tritons than deuterons or ^{3}He. The targets were carefully weighed, the thickness values being confirmed by α particle energy-loss measurements for the two thinnest targets with an uncertainty evaluated to be 4%.

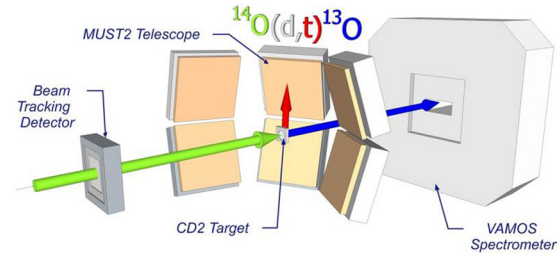

FIG. 1. Experimental setup with the MUST2 array and VAMOS spectrometer.

The MUST2 array [32] was dedicated to the detection and identification of light charged particles (Fig. 1): four telescopes at forward angles for tritons and ^{3}He and a wall of two telescopes at 90° relative to the beam axis for elastically scattered deuterons. The telescopes consisted of two stages: (i) a 300 μm thick double-sided silicon strip detector (DSSSD), 10×10 cm^2, with 128 horizontal and vertical strips; (ii) an additional 4.5 mm thick Si-Li detector for the wall at 90°; or (iii) an additional layer of 40 mm thick trapezoidal CsI scintillators at forward angles. The distance between the target and the forward telescopes was 18 cm, resulting in an angular resolution of 0.2°. Particles stopped in the DSSSD stage (all ^{3}He and the low-energy deuterons) were identified in mass by a time-of-flight measurement. For particles punching through the DSSSD stage, full identification was carried out by the ΔE-E technique [Fig. 2(a)]. For an exclusive discrimination, ejectiles were identified in the focal plane of the VAMOS magnetic spectrometer [33] with the usual setup: two position-sensitive drift chambers for Bρ and angle reconstruction, an ionization chamber, and a plastic scintillator for energy-loss and time-of-flight measurements from which mass and atomic number were determined. Two beam-tracking detectors [34] before the target, set one meter apart from each other, were used to reconstruct the beam profile at the target position and improve the overall angular resolution. The reference for the time-of-flight measurements was given by one of the beam tracking detectors. The detection of ejectiles was constrained by the angular acceptance of the VAMOS spectrometer, limited here to ±4.2° in the laboratory frame. A typical two-dimensional (2D) plot of the energy of the tritons as a function of their detection angle is shown in Fig. 2(b) after selection of ^{13}O in VAMOS.

For ^{16}O and ^{18}O, we analyzed in addition the following previously published angular distributions:

(i) $^{16}\mathrm{O}(d,{}^3\mathrm{He})^{15}\mathrm{N}$ at 26 MeV/nucleon [35] populating both the $1/2^-$ ground state and the 6.32-MeV $3/2^-$ state;
(ii) $^{16}\mathrm{O}(d,t)^{15}\mathrm{O}$ at 14 MeV/nucleon [36] to the ground state;
(iii) $^{18}\mathrm{O}(d,{}^3\mathrm{He})^{17}\mathrm{N}$ at 26 MeV/nucleon [37] to the ground state.

These data, together with those of Ref. [31], cover a large range of ΔS values with few significant gaps.

[1] p, d, and t are used as standard abbreviations for proton (^{1}H), deuteron (^{2}H), and triton (^{3}H), respectively.

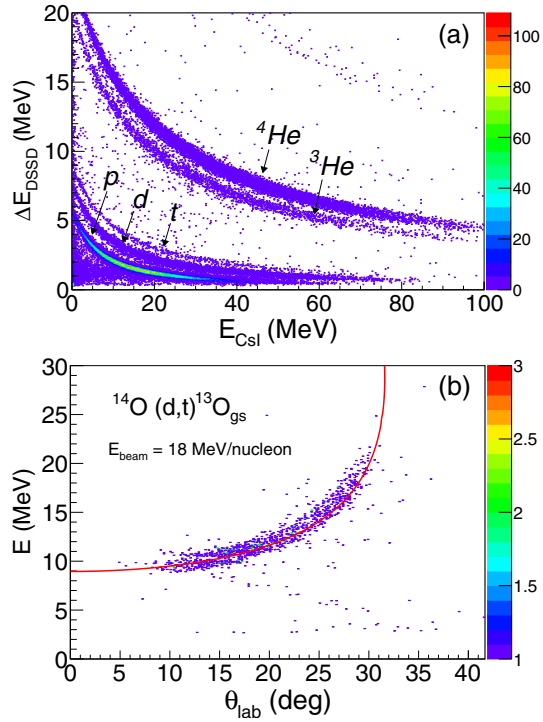

FIG. 2. Identification of reaction channels with the MUST2 array and VAMOS spectrometer: (a) ΔE-E identification with MUST2 (DSSSD-CsI) for light particles punching through the DSSSD detector; (b) 2D plot of the energy of tritons detected in MUST2 as a function of their detection angle in the laboratory frame gated on the detection of ^{13}O in the focal plane of VAMOS. The kinematics of the ^{14}O(d,t) transfer reaction to the ground state of ^{13}O is superimposed as the red line.

III. DATA ANALYSIS

A. Reaction framework

For the bulk of our analysis of the single-nucleon stripping reactions we used the coupled reaction channels (CRC) approach since it treats all reaction processes on the same footing and makes the least number of approximations of any reaction formalism implemented in readily available codes. We also performed distorted wave Born approximation (DWBA) calculations, discussed in Sec. III D, to get a grasp on the effects of including explicitly coupling to the deuteron breakup and not treating the transfer couplings as perturbations. Detailed descriptions of the DWBA and CRC formalisms may be found in standard texts on direct reactions, e.g., Ref. [16], so we provide only necessary details of the inputs to our calculations here.

All calculations were performed with the code FRESCO [38]. In the main set of calculations couplings to the deuteron breakup and single-nucleon pick-up reactions were included using the coupled discretized continuum channels (CDCC) [39] and CRC approaches, respectively. The coupling schemes used in the ^{14,16}O analyses are shown in Fig. 3. The CDCC procedure was similar to to that described in Ref. [40]. The continuum was divided into bins in momentum (k) space of width $\Delta k = 0.125$ fm^{-1} up to a maximum value $k_{\max} =$

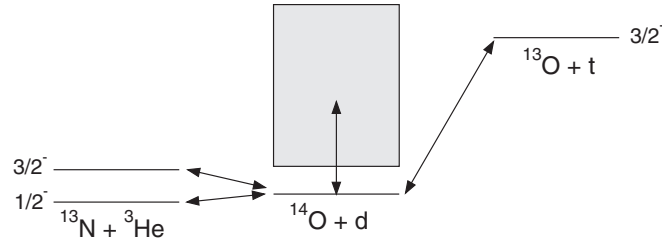

FIG. 3. Coupling scheme used in the CRC calculations of the single-nucleon pick-up for ^{14}O.

0.75 fm^{-1} for the 18.1 MeV/nucleon ^{14}O and 14 MeV/nucleon ^{16}O data and $k_{\max} = 1.0$ fm^{-1} for the 26 MeV/nucleon ^{16,18}O data. The transfer steps included full complex remnant terms and nonorthogonality corrections.

B. Optical potentials

The entrance channel deuteron-nucleus potentials in the CRC calculations were constructed by Watanabe-type folding of the central part of global nucleon-nucleus optical potentials over the deuteron internal wave function. The latter was calculated using the Reid soft-core nucleon-nucleon interaction [41]. The coupling potentials for the deuteron breakup were calculated in the same way. We performed calculations based on four different sets of global nucleon-nucleus optical potential parameters [42–45] in order to investigate the influence of the entrance channel potential on the calculated pick-up cross sections. In each case the real and imaginary parts of the potentials were renormalized by factors λ_V and λ_W, respectively, to obtain optimum agreement with the elastic scattering data. For the 52 MeV $d + ^{18}$O calculations no elastic scattering data are available so the same λ_V and λ_W values as for the corresponding $d + ^{16}$O calculations were used. Typical results of CRC calculations based on each of the four potentials are compared with the deuteron elastic scattering data in Fig. 4.

By contrast with the entrance channel no data are available for the elastic scattering in the exit channels and such measurements are well beyond the scope of most experiments due to the lack of appropriate ^{3}H and ^{3}He targets. In Ref. [31] we used two different t- and ^{3}He-nucleus optical model potentials, the systematics of Becchetti and Greenlees (BG) [47] (tabulated in Ref. [48]) and the GDP08 optical potential for $A = 3$ projectiles [49]. The BG potential [47] was obtained by a systematic study in the region $A > 40$ and $E_{\rm inc} < 40$ MeV. GDP08 was derived from fitting a set of angular distributions for ^{3}He elastic scattering on targets with $40 \leqslant A \leqslant 209$ and incident energies $30 \leqslant E_{\rm inc} \leqslant 217$ MeV. The resulting potential reproduces the elastic scattering of both ^{3}He and ^{3}H nuclei. While the potentials of Refs. [47,49] are outside their strict range of validity for the cases we are interested in they nevertheless provide reasonable descriptions of ^{3}H and ^{3}He $+^{12,13}$ C elastic scattering data in the same incident energy region. Since Ref. [31] was published a further set of global parameters for $A = 3$ projectiles has become available, HT1p [50], specifically adapted to targets in the 1p shell. We have therefore performed in this work an

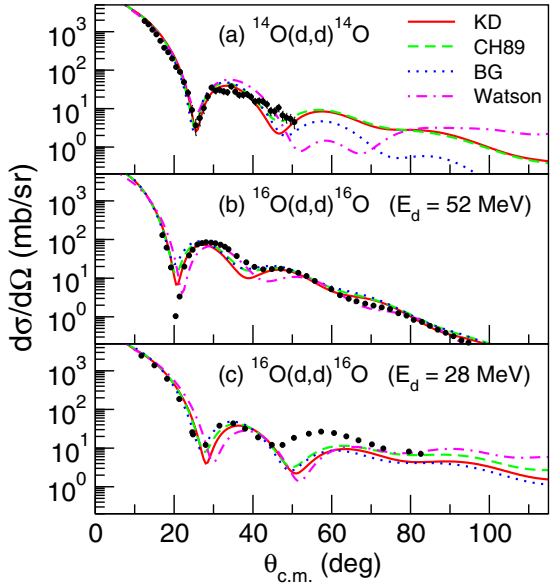

FIG. 4. Elastic scattering angular distributions for: (a) $^{14}O + d$ at $E_d = 36$ MeV [31], (b) $^{16}O + d$ at $E_d = 52$ MeV [46], (c) $^{16}O + d$ at $E_d = 28$ MeV [36]. The curves denote the results of CRC calculations based on four different input potentials: Koning and Delaroche [42] (solid red line), CH89 [44] (dashed green line), Becchetti and Greenlees [43] (dotted blue line), and Watson *et al.* [45] (dot-dashed magenta line). In all cases the exit channel potentials were calculated using the GDP08 [49] parameters.

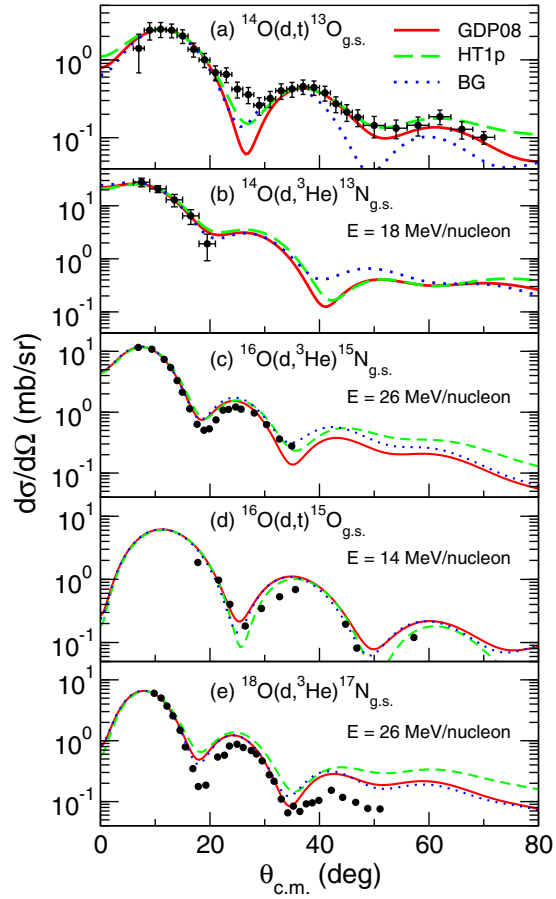

FIG. 5. Results of CRC calculations based on the parameters of Ref. [42] in the entrance channel and each of the potentials of Refs. [47,49,50] in the exit channels compared with the data for: (a) the $^{14}O(d,t)^{13}O$ reaction at 18 MeV/nucleon [31] (b) the $^{14}O(d,^3He)^{13}N$ reaction at 18 MeV/nucleon [31] (c) the $^{16}O(d,^3He)^{15}N$ reaction at 26 MeV/nucleon [35] (d) the $^{16}O(d,t)^{15}O$ reaction at 14 MeV/nucleon [36], and (e) the $^{18}O(d,^3He)^{17}N$ reaction at 26 MeV/nucleon [37].

additional set of calculations using this potential in the exit channels.

In Fig. 5 we compare the results of CRC calculations based on the Koning and Delaroche optical potential parameters [42] in the entrance channel and each of the potentials of Refs. [47,49,50] in the exit channels with the data for the $^{14}O(d,t)^{13}O_{g.s}$ and $^{14}O(d,^3He)^{13}N_{g.s}$ reactions at 18 MeV/nucleon [31], the $^{16}O(d,^3He)^{15}N_{g.s}$ reaction at 26 MeV/nucleon [35], the $^{16}O(d,t)^{15}O_{g.s}$ reaction at 14 MeV/nucleon [36] and the $^{18}O(d,^3He)^{17}N_{g.s}$ reaction at 26 MeV/nucleon [37]. The description of the $^{14}O(d,^3He)^{13}N$ data is similar for all three exit channel potentials and the predictions at larger angles ($20^\circ \leqslant \theta_{c.m.} \leqslant 80^\circ$) are not significantly different. However, the description of the $^{14}O(d,t)^{13}O$ data by the calculation using the potential parameters of Ref. [47] in the exit channel is noticeably worse for angles $\theta_{c.m.} > 35^\circ$. For the $d + ^{16}O$ system all three exit channel potentials give similar descriptions of the data, significant differences only appearing in the predictions for the $^{16}O(d,^3He)^{15}N$ reaction at 52 MeV for angles $\theta_{c.m.} > 35^\circ$ where there are no data. For the $d + ^{18}O$ system the exit channel potentials of Refs. [47] and [49] give similar good descriptions of the data, while the more recent potential of Ref. [50] gives a noticeably poorer result.

C. Overlap functions

The overlap functions (OFs) are key elements in calculating transfer reaction cross sections since they contain the information about the structure of the nuclei involved. Any structure model can in principle calculate these overlaps keeping in mind that the asymptotic behavior can be especially important due to the peripherality of most direct reactions. Although these OFs are typically calculated as single-particle solutions of a Woods-Saxon (WS) mean-field potential it is now also possible to use the results of *ab initio* calculations. Both alternatives have to be used with caution: (i) a WS solution has the proper asymptotic behavior by construction but its amplitude in the peripheral region probed by the reaction depends strongly on the geometry of the potential used to generate it, particularly the radius parameter; (ii) while an *ab initio* calculation can provide a consistent overlap function and spectroscopic factor (normalization) it may have difficulty in producing simultaneously a realistic asymptotic behavior [51]. It should also be underlined that in full finite-range calculations, as here, there are two overlap functions to be considered for a given partition, the targetlike and the projectilelike (the latter being replaced by a normalization factor in the zero-range approximation). In this section we investigate the impact of using $\langle ^AO \mid ^{A-1}O + n\rangle$ and $\langle ^AO \mid ^{A-1}N + p\rangle$ OFs calculated

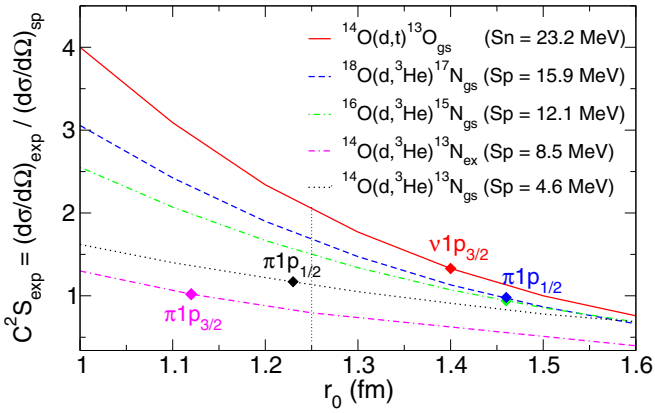

FIG. 6. Dependence of C^2S_{exp} on r_0 for the different transfer reactions involved in this study. All the transferred particles have angular momentum $\ell = 1\hbar$ relative to their respective core nuclei. The values are the results of CRC calculations based on the same optical potential parameter sets for the entrance [42] and exit [49] channels. The diamonds denote the values of r_0 used in the present analysis, which reproduce the rms radii of the HFB calculations. A vertical dashed line is shown to indicate the values of C^2S_{exp} obtained with the conventional choice of $r_0 = 1.25$ fm.

in the usual way using WS potential wells versus those obtained from *ab initio* calculations (described briefly in Ref. [31]). We also check the influence of two different choices for the $\langle {}^3\mathrm{H} \mid {}^2\mathrm{H} + n\rangle$ and $\langle {}^3\mathrm{He} \mid {}^2\mathrm{H} + p\rangle$ projectilelike OFs.

As we have already noted, the OFs are typically calculated using wave functions for a nucleon bound in a WS well of radius $R_0 = r_0 \times A^{1/3}$ fm and diffuseness a_0 fm where A is the mass number of the core nucleus, with the depth adjusted to reproduce the experimental single-nucleon separation energy. Usually reasonable values are chosen for the parameters of the WS well, a popular choice being $r_0 = 1.25$ fm and $a_0 = 0.65$ fm, based on early optical model analyses of nucleon elastic scattering [18–20]. However, as Satchler [16] points out, while "not unreasonable, and hallowed by usage, these parameter values are essentially arbitrary" and additional constraints on r_0 are necessary. To quantify the importance of such constraints, we first show in Fig. 6 the dependence of the experimental spectroscopic factor C^2S_{exp} on the reduced radius r_0 for the overlaps of interest here. All the transferred particles have angular momentum $\ell = 1\hbar$ relative to their respective core nuclei. The slope of C^2S_{exp} as a function of r_0 tends to increase with the separation energy of the transferred particle. In the most sensitive case, ^{14}O(d,t), a linear fit gives $\Delta C^2S_{exp} \approx 5 \times \Delta r_0$ and impacts the uncertainty in the absolute value of C^2S_{exp}. The dependence is much reduced for the $(d,{}^3\mathrm{He})$ channel with $\Delta C^2S_{exp} \approx 1.6 \times \Delta r_0$. Obviously the exact extent of the uncertainty due to the choice of r_0 for a given case will depend on the range of values considered reasonable. Also, this choice need not necessarily be the same for all states. This sensitivity, together with the fact that the overall shape of the calculated angular distributions is nearly unaffected by the variation of r_0, confirm that some additional physical constraints on this parameter are desirable.

TABLE I. Rms radii of the $1p_{3/2}$ and $1p_{1/2}$ orbitals obtained from HFB calculations with the SLy4 interaction [53] for ^{14}O, ^{16}O, and ^{18}O. In the last row the rms radii for the $1/2^-$ ground state and 6.32 MeV $3/2^-$ excited state of ^{15}N obtained from a quasielastic proton knockout measurement [52] are given for comparison.

HFB RMS (fm)	$\pi 1p_{3/2}$	$\pi 1p_{1/2}$	$\nu 1p_{3/2}$	$\nu 1p_{1/2}$
^{14}O	2.77	3.03	2.69	2.72
^{16}O	2.80	2.95	2.78	2.91
^{18}O	2.81	2.91		
^{16}O$(e,e'p)^{15}$N	2.719(24)	2.943(30)		

For protons, the rms radius of the bound-state wave function may be obtained from quasielastic proton knockout measurements. The rms radii of the $1/2^-$ ground and $3/2^-$ first excited states of ^{15}N, 2.943(30) fm and 2.719(24) fm, respectively, are known from an analysis of ^{16}O$(e,e'p)$ data [52]. Both states have a strong single-particle character, $\pi 1p_{1/2}$ and $\pi 1p_{3/2}$, respectively. The rms radii are reproduced by WS potential wells of diffuseness $a_0 = 0.65$ fm and $r_0 = 1.46$ fm and 1.31 fm, respectively (spin-orbit terms of depth 9 MeV and the same geometry as the central parts were also included in the potentials). The same r_0 value was adopted for the corresponding neutron wave function for the ^{15}O ground state.

With no $(e,e'p)$ data available for ^{14}O and ^{18}O we performed Hartree-Fock-Bogoliubov (HFB) calculations with different Skyrme interactions to fix the radii of the $\pi 1p_{3/2}$ and $\pi 1p_{1/2}$ wave functions in these nuclei. The results for the Sly4 interaction [53] are given in Table I. Fair agreement is obtained with the values extracted from the ^{16}O$(e,e'p)$ analysis for the ^{15}N $1/2^-$ and $3/2^-$ states [52]. We therefore used these radii for the $0p$ wave functions from the HFB calculations as a further constraint on the corresponding r_0 values of the WS potential used to generate OFs in the CRC calculations (see Table I of Ref. [31]). Similar calculations were performed with other Skyrme interactions with results always in agreement with the ^{16}O$(e,e'p)$ values, from which we deduced the variance in r_0 used in Ref. [31].

In almost all cases the difference between the adopted value of r_0 and the standard value of 1.25 fm is significant. As Fig. 6 shows, this can have important consequences for the value of C^2S_{exp} obtained. The most important difference is for the ^{14}O$(d,t)^{13}$O$_{gs}$ reaction where the adopted value of r_0, 1.40 fm, is a 12% increase over 1.25 fm and leads to a reduction in C^2S_{exp} from 2.10 to 1.35, a factor of ∼36%, see Fig. 6.

In Ref. [31] we also performed calculations with OFs obtained from *ab initio* calculations using the self-consistent Green's function (SCGF) theory [54,55]. This approach provides an alternative means of constraining the OFs used in transfer reaction calculations but its use in reaction calculations also presented some difficulties. First, it was shown that the chiral N3LO(2NF) + NNLO(3NF) interactions available at that time lead to calculated charge radii systematically smaller than the experimental one, by about 0.2 fm for ^{16}O [55]. The microscopic OFs were thus all rescaled in coordinate space by the same factor (one phenomenological correction) to account for this difference. Although it goes beyond the scope of this

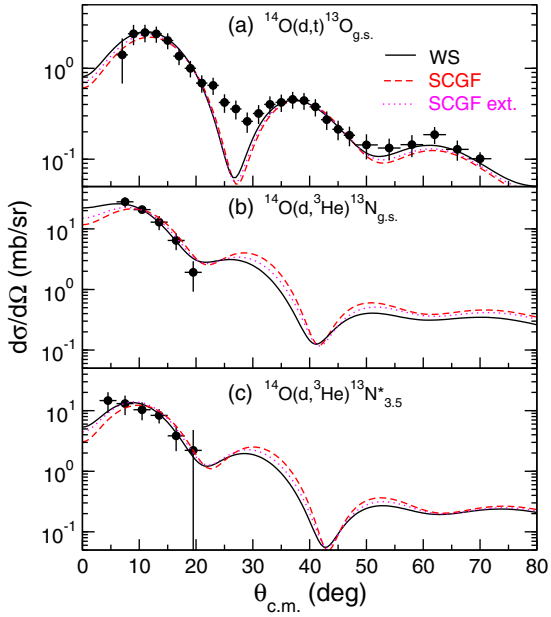

FIG. 7. Angular distributions for: (a) the ^{14}O(d,t) and (b) and (c) the ^{14}O$(d,^3$He) transfer reactions at 18 MeV/u [31]. Calculations were performed with different prescriptions for the $\langle^{14}\text{O} \mid {}^{13}\text{O}+n\rangle$ and $\langle^{14}\text{O} \mid {}^{13}\text{N}+p\rangle$ OFs: WS (solid red curve), SCGF (dashed green curve), and extrapolated SCGF (dotted blue curve). The curves are the results of CRC calculations based on the same optical potential parameter sets for the entrance [42] and exit [49] channels.

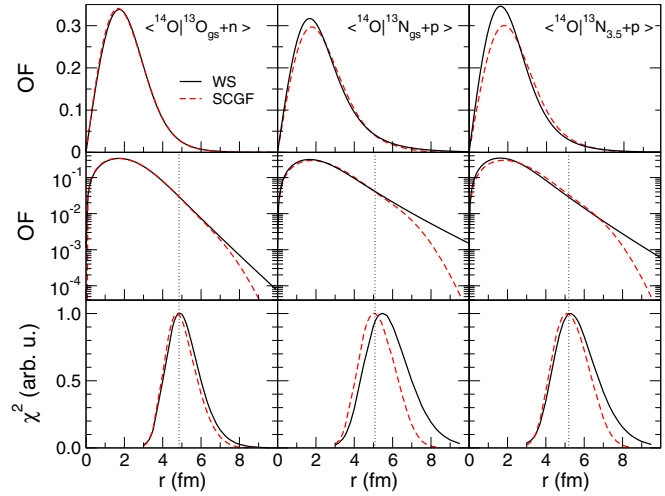

FIG. 8. Overlap functions on linear and log scale (top and middle rows) for the $\langle^{14}\text{O} \mid {}^{13}\text{O}+n\rangle$ (left column), $\langle^{14}\text{O} \mid {}^{13}\text{N}+p(1\text{p}_{1/2})\rangle$ (middle column), and $\langle^{14}\text{O} \mid {}^{13}\text{N}+p(1\text{p}_{3/2})\rangle$ (right column). For each case two prescriptions for the OF (described in the text) are shown: Woods-Saxon (black line), SCGF (dashed red line). Bottom row: Notch tests performed for each channel as a function of the radius (see text for details).

study, note that this deficiency has been extensively studied since our initial work (see Ref. [56] and references therein) and is mostly resolved by new fits of chiral interactions that were also constrained by the experimental charge radii of ^{16}O [57]. Second, as can be seen in Fig. 8, the asymptotic behavior of these OFs is not physical, their decay as a function of radius being much faster than the expected exponential for radii greater than $\sim$ 6 fm. This limitation resulted from the use of a harmonic oscillator basis to expand the OFs and it is also resolved in more recent studies [58].

The unphysical tail of the OFs may be a problem since transfer reactions are usually considered to be mainly peripheral and sensitive to the external part of the wave functions. Since these OFs were used without modification in Ref. [31] we present here the results of tests performed to quantify the impact of the incorrect asymptotic behavior of the SCGF OFs on the transfer angular distributions calculated with them. Exponential fits to the OFs for radii between 4.0 and 6.5 fm were extrapolated out to a radius of 30 fm and used to replace the SCGF OFs for radii greater than 6.5 fm. The results of calculations using these extrapolated SCGF OFs are compared with those using the original OFs and our WS OFs in Fig. 7.

The effect on the shape of the angular distributions is not significant but the use of the extrapolated SCGF OFs does occasionally lead to small differences in the C^2S_{exp} values. However, these are usually much smaller than those due to the effect of using different input optical potentials and are well within the uncertainties given in Ref. [31]. Thus, in this particular case we conclude that the incorrect asymptotic behavior of the SCGF OFs does not affect the reaction calculation, suggesting that it is not particularly sensitive to the OFs in the radial region $r > 6.5$ fm.

In order to test this conclusion as to the radial sensitivity we performed a notch test [59] where a Gaussian shape notch of central value equal to 0 was removed from the $\langle^{14}\text{O} \mid {}^{13}\text{O}+n\rangle$ and $\langle^{14}\text{O} \mid {}^{13}\text{N}+p\rangle$ OFs one at a time and the effect on the respective calculated angular distribution observed. The width of the notch was smaller than the distance between the points so that the region of sensitivity could be precisely tested (in fact, it was found that the exact width of the notch did not affect the result). To provide an objective quantification of the effect we defined a χ^2 value as:

$$\chi^2 = \Sigma((d\sigma/d\Omega)_{\text{pert}} - (d\sigma/d\Omega)_{\text{un}})^2/(d\sigma/d\Omega)^2_{\text{un}}, \qquad (1)$$

where the $(d\sigma/d\Omega)_{\text{pert,un}}$ are the perturbed and unperturbed calculated cross sections, respectively, at a given angle and the sum is over the angles. Calculations were performed for both WS and SCGF OFs. The angular range used to calculate χ^2 was restricted to the first oscillation, that is $5^\circ \leqslant \theta_{\text{c.m.}} \leqslant 20^\circ$ for ^{14}O$(d,^3$He) and $8^\circ \leqslant \theta_{\text{c.m.}} \leqslant 30^\circ$ for ^{14}O(d,t). The results are shown in Fig. 8. The region of sensitivity is similar in all cases, peaking at $\sim$ 5 fm, and is noticeably wider for the $(d,^3$He) channels, perhaps due to the influence of the Coulomb force on the proton, with a slightly greater degree of peripherality compared to the (d,t) channel. Figure 8 clearly demonstrates why the incorrect asymptotic behavior of the SCGF OFs has such a small influence on the calculated angular distributions in this case.

In addition, we also investigated the influence of a different choice of OFs for the light particle vertices involved in the reactions, namely $\langle^3\text{H} \mid d+n\rangle$ and $\langle^3\text{He} \mid d+p\rangle$. All the C^2S_{exp} values given in Table I of Ref. [31] were obtained

using the prescriptions given in Ref. [60] for these OFs. We therefore determined the C^2S_{exp} using a different prescription for these OFs, that of Ref. [61], employing the same procedure as in Ref. [31]. The C^2S_{exp} values extracted with these light particle vertices are larger than those given in Ref. [31] by a global factor of about 1.4 for all the systems investigated here, thus a different choice of this input merely scales the result of Ref. [31] by a single factor and does not affect the conclusions.

Finally, it is worth noting that reaching a consistent description of radial overlap functions is also crucial for the interpretation of other peripheral direct reactions such as knockout at intermediate energies for which similar studies were performed using either standard or *ab initio* inputs [23,62] but also for $(p,2p)$ reactions at higher energies [63]. This is particularly important when trying to compare results obtained with different probes and interpreted with different reaction formalisms, such as the dependence of the valence correlations as a function of the difference in separation energy further discussed in Sec. IV of this paper.

D. CRC vs DWBA

We also compared our CRC calculations to the results of a standard DWBA analysis using the same Woods-Saxon OFs. We chose the CRC calculations based on the optical potential sets of Refs. [42] and [49] in the entrance and exit channel, respectively, for this comparison while the DWBA calculations used the potentials of Refs. [64] and [49] in the entrance and exit channels, respectively. Figure 9 and Table II compare the results. The shapes of the experimental angular distributions are globally well reproduced by both sets of calculations in all cases except for the $^{14}O(d,t)$ DWBA calculation at large angles. The differences in the extracted spectroscopic factors C^2S_{exp} vary from one channel to another and no global tendency is observed between the two calculations. The largest difference in $\delta = (C^2S_{exp}^{CRC} - C^2S_{exp}^{DWBA})/C^2S_{exp}^{DWBA}$ is also observed for the $^{14}O(d,t)$ reaction, see Table II. The use of DWBA rather than CRC (including explicitly coupling to the deuteron breakup) thus appears to introduce random changes in the C^2S_{exp} values leading to a larger uncertainty, even when the inputs to the two sets of calculations are as similar as possible.

IV. RESULTS

In this section we discuss in more detail than was possible in Ref. [31] the results of the individual CRC calculations. We also give the results of new CRC calculations performed using the HT1p optical potential parameter set of Ref. [50] in the exit channels, specifically adapted to target nuclei in the 1p shell, which has become available since our original analysis was performed. Tables giving the values of C^2S_{exp} for each of the CRC calculations with the various combinations of optical potentials and OFs are supplied in the Supplemental Material [65].

In Fig. 10 we plot as a function of ΔS the reduction factor R_s values for CRC calculations using the WS OFs and based on each of the four sets of global nucleon-nucleus optical potentials in the entrance channels and the three exit channel optical potentials in turn. The lines on the figure denote the results of straight line fits to the experimental R_s values. The results for

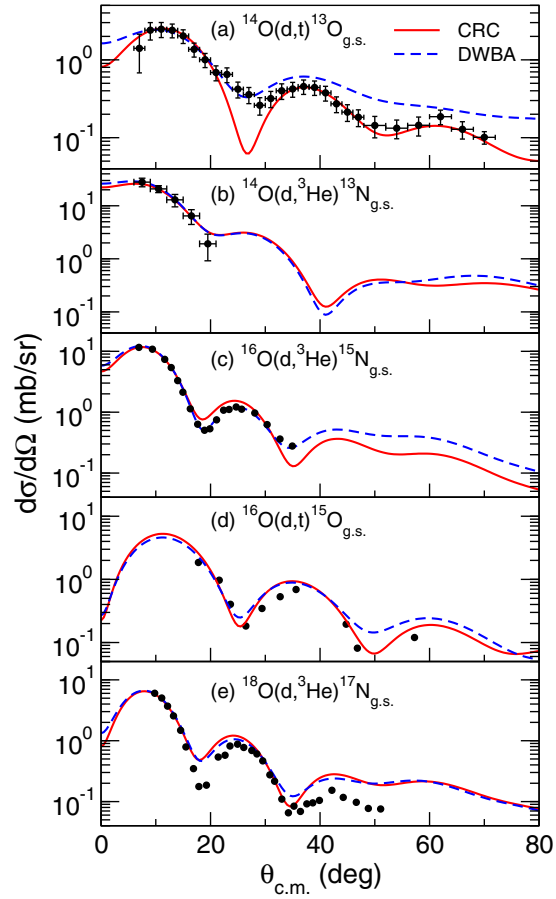

FIG. 9. Comparison of DWBA (dashed blue) and CRC (solid red) calculations for the single-nucleon stripping reactions. Reaction energies are the same as in Fig. 5. See text for the choice of potentials.

calculations using the SCGF OFs in either unaltered or extrapolated form are similar, differing only in matters of detail.

The first point to note is that the calculations based on the optical potential parameters of Watson *et al.* [45] in the entrance channel give rise to R_s values, which are, except

TABLE II. C^2S_{exp} values extracted from the CRC calculations based on the potentials of Refs. [42] and [49] in entrance and exit channels, respectively and from DWBA analysis. The DWBA calculations used the same exit channel optical potential parameters and OFs as the CRC calculations and the deuteron optical model parameters of Ref. [64] in the entrance channel. The final column is the variation normalized to the DWBA result.

Reaction	E^*	r_0	C^2S_{exp}		$\delta(C^2S_{exp})$
	(MeV)	(fm)	CRC	DWBA	%
^{14}O(d,t)^{13}O	0.0	1.40	1.35	1.00	35
^{14}O(d,^{3}He)^{13}N	0.0	1.23	1.15	1.31	−12
	3.5	1.12	1.02	0.90	12
^{16}O(d,^{3}He)^{15}N	0.0	1.46	0.94	0.94	0
	6.3	1.31	2.00	1.70	18
^{18}O(d,^{3}He)^{17}N	0.0	1.46	0.95	0.90	6

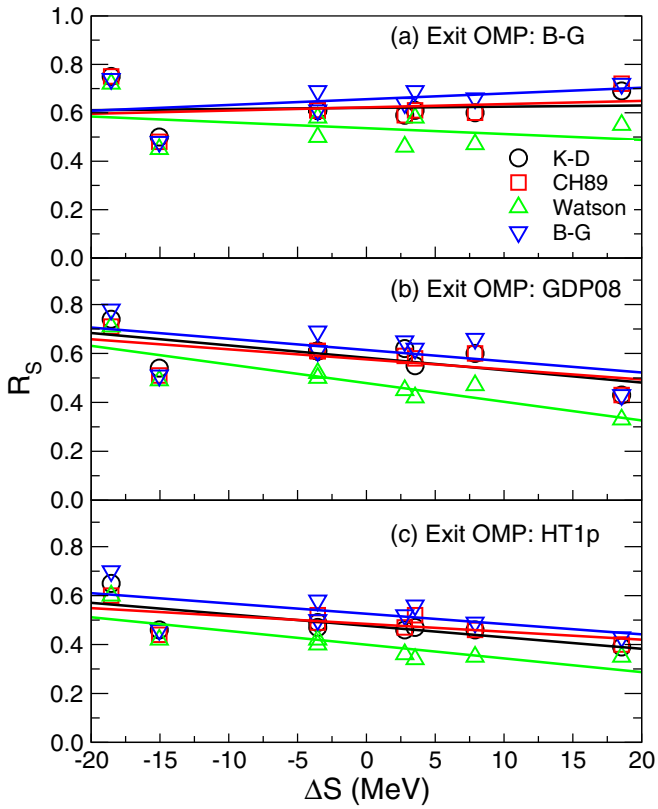

FIG. 10. Reduction factor R_s values obtained from CRC calculations with WS OFs and exit-channel optical model potentials: (a) B-G from Ref. [47], (b) GDP08 from Ref. [49], and (c) HT1p from Ref. [50]. The symbols correspond to the use of different input-channel optical model potentials and the lines denote linear fits to the corresponding R_s sets.

for the two ^{14}O$(d,^3$He$)^{13}$N points ($\Delta S \approx -20$, -15 MeV), significantly smaller than those obtained when using the other three sets of parameters [42–44]. This may be due to the fact that the parameters of Watson *et al.* [45] were tuned to fit nucleon scattering data from targets in the 1p shell and therefore take into account influences of the specific nuclear structure of these nuclei that make them less suitable as inputs to the folding procedure adopted to obtain our deuteron potentials than the true global parameter sets of Refs. [42–44]. The second point is that the ^{3}H optical potential parameters of Ref. [47] give a consistently higher value of R_s for the ^{14}O$(d,t)^{13}$O data ($\Delta S \approx 20$ MeV) than the other two exit channel potentials. Thus, the exact variation of R_s as a function of ΔS obtained from an analysis of this data set will depend on the choice of optical potential parameters even for a fixed set of OFs. However, it is possible to state with confidence that any variation in R_s is small; the slopes of the straight line fits to each of the different sets of determinations shown on Fig. 10 vary from $+0.0024$ MeV^{-1} to -0.0076 MeV^{-1}. These values are slightly higher than that obtained in Ref. [31] for the WS OFs due to the averaging procedure used in that work leading to a certain amount of cancellation between the ^{14}O$(d,t)^{13}$O points for analyses performed with the potential of Ref. [47] in the exit channels and those using the potential of Ref. [49]. Nevertheless, the conclusions of that work remain unchanged.

In Fig. 11 we provide in graphical form a more general summary of the results of the individual determinations, presented as the percentage deviation of the extracted spectroscopic factors C^2S_{exp} from the mean values given in Ref. [31]. The figure is arranged as follows. Each of the five columns represents a single data set; in order to keep the figure within reasonable limits we have omitted the 28 MeV ^{16}O$(d,^3$He$)^{15}$N and 52 MeV ^{18}O$(d,^3$He$)^{17}$N data. The central solid line in each column (labeled "0" on the figure) represents the mean C^2S_{exp} value given in Ref. [31] while the dotted vertical lines represent the values obtained from CRC calculations based on the potential parameters of Ref. [42] in the entrance channel, the potential parameters of Ref. [49] in the exit channels and with WS OFs calculated using the radius values given in Table I, which we have used as our reference in producing the figure. The various rows show the effect of making different choices for a given type of input to the calculations, while other ones are kept identical.

The first four rows demonstrate the influence of the choice of entrance channel potential parameters on the values of C^2S_{exp} obtained. The labels KD, CH89, BG, and WAT denote CRC calculations with entrance channel potentials based on the parameters of Refs. [42], [44], [43], and [45], respectively. The yellow bars indicate the percentage deviation of the C^2S_{exp} from the respective mean values of Ref. [31].

The next two rows, labeled GDP08 and BG represent CRC calculations with entrance channel potentials based on the parameters of Ref. [42], WS OFs calculated with the radii of Table I and the potential parameters of Refs. [49] and [47], respectively, in the exit channels. The cyan bars represent the percentage deviation of the C^2S_{exp} from the respective mean values of Ref. [31].

The next six rows, labeled WS(SLy4) to SCGF(2) represent different choices for the OFs: WS(SLy4) denotes OFs calculated using WS potential wells with radii consistent with HFB calculations using the SLy4 interaction, WS(SkX) OFs calculated using WS wells with radii consistent with the results of HFB calculations using the SkX interaction, WS(SkM*) OFs calculated using WS wells with radii consistent with the results of HFB calculations using the SkM* interaction, WS(1.25 fm) OFs calculated using WS wells with $r_0 = 1.25$ fm, SCGF(1) the unmodified SCGF OFs, and SCGF(2) the SCGF OFs with extrapolated tails. All these calculations used entrance channel potentials based on the parameters of Ref. [42] and the exit channel potential parameters of Ref. [49]. The green bars denote the percentage deviation of the C^2S_{exp} from the respective mean values of Ref. [31].

The final two rows illustrate the effect of using DWBA rather than CRC to model the reaction mechanism. Both CRC and DWBA calculations employ identical OFs and exit channel potentials while the CRC calculation entrance channel potentials are based on the parameters of Ref. [42] and the DWBA calculations employ the deuteron optical potential of Ref. [64]. The red bars represent the percentage deviation of the C^2S_{exp} from the respective mean values of Ref. [31]. In each set of comparisons the rows labeled in bold text denote the reference calculation, repeated for the sake of convenience.

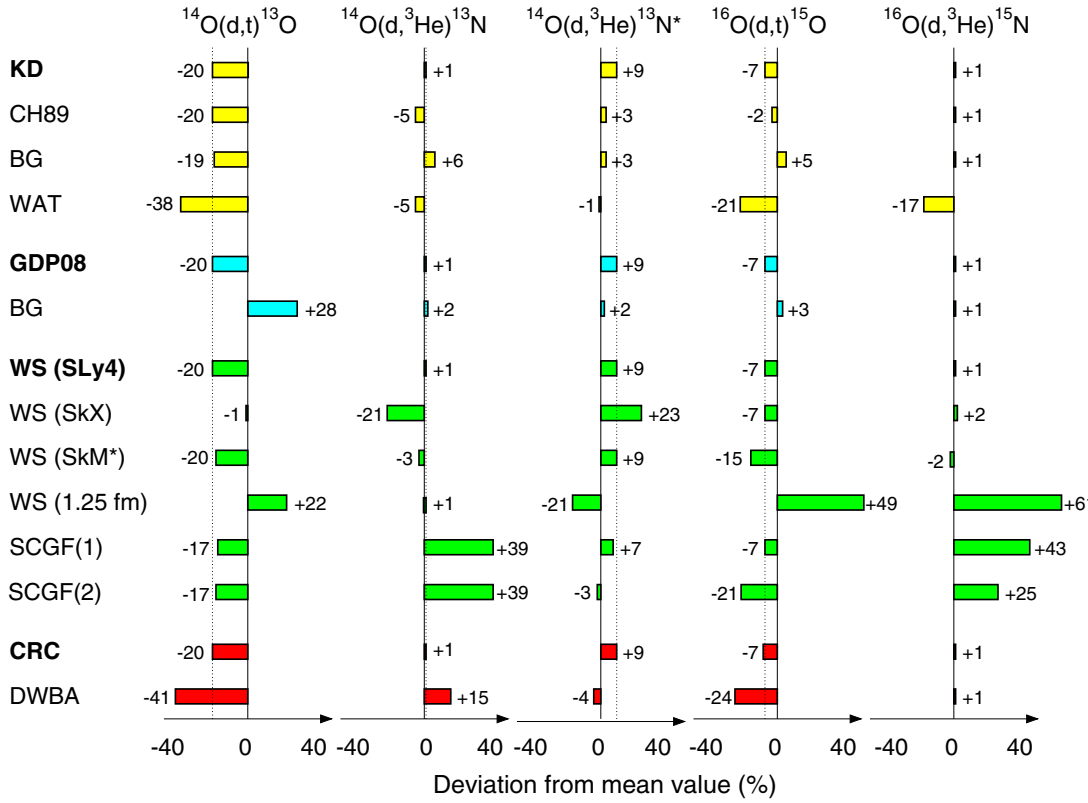

FIG. 11. Percentage deviations of C^2S_{exp} from the mean values of Ref. [31] as a function of different analysis input choices. See text for details.

It is immediately apparent from Fig. 11 that the use of entrance channel potentials based on the parameters of Watson *et al.* [45] in most cases leads to C^2S_{exp} values significantly different from those obtained from calculations based on the other parameter sets used in this study, underlining the conclusion drawn from Fig. 10. The other observation, again in accordance with our conclusions from Fig. 10, is that while the exit channel potentials of Refs. [47] and [49] in general yield C^2S_{exp} values in good agreement there is a significant difference for the ^{14}O$(d,t)^{13}$O case. Figure 11 also clearly demonstrates that the choice of OFs has the greatest influence on the C^2S_{exp} values and that this influence is not systematic but rather random, at least for this data set. Finally, the use of DWBA rather than CRC introduces random differences in the C^2S_{exp} values, as already noted in the discussion of Table II. We note that for the ^{16}O(d,t) data at 28 MeV and, to a lesser extent, the ^{16}O$(d,^3$He) data at the same energy the differences in C^2S_{exp} values obtained in the CRC and DWBA calculations are the result of a more or less subjective judgement. The result depends on which angular region of the data is used for the normalization of the theoretical curves since the measurements of Ref. [36] do not extend to small enough angles to define the first peak of the angular distribution.

V. CONCLUSION

We have presented the results of an extended study to quantify the influence of different choices of input to CRC calculations on the C^2S_{exp} values extracted from a data set covering the ^{14}O(d,t), ^{14}O$(d,^3$He), ^{16}O(d,t), ^{16}O$(d,^3$He), and ^{18}O$(d,^3$He) reactions, with particular reference to the reduction factor (R_s) study of Ref. [31]. The most important conclusion is that the main result of Ref. [31], the lack of a significant variation of R_s with ΔS, the single-nucleon separation energy asymmetry, does not depend on these choices. The influence of a particular set of choices of entrance and exit channel potentials and OFs on this result is confined to matters of detail such as the exact value of the slope of a straight line regression fit to the R_s values, which remains small ($\leqslant$0.01 MeV^{-1}) for all the various combinations investigated here. This conclusion is incompatible with the large R_s slope extracted from knockout data at intermediate energy [23,24] but in agreement with the one extracted very recently using $(p,2p)$ reactions on oxygen isotopes at higher energy [63]. This apparent incompatibility for large ΔS remains a subject of debate and possible deficiencies in the reaction model used to describe either transfer or knockout reactions should continue to be investigated carefully. For example, the basic factorization procedure used to extract experimental spectroscopic factors $\sigma_{exp} \propto C^2S_{exp} \times \sigma_{sp}$ may also be inadequate for some of these reactions, especially on very asymmetric nuclei, hindering the definition of a consistent and common quantity directly comparable for different types of reactions.

Concerning the variance of R_s values for a particular transfer data set, it should be noted that certain choices of input parameters can lead to extreme values. For example, it is apparent that the use of entrance channel potentials based on the parameters of Ref. [45] leads in most cases to

significantly different values to those obtained with the three other parameter sets investigated in this study. Also, for the ^{14}O$(d,t)^{13}$O case only, the exit channel potentials using the parameters of Refs. [47] and [49] give significantly different R_s values, ranging from 0.33–0.72 for geometry constrained WS OFs, a fact that was somewhat masked in Ref. [31] by the averaging procedure used. This range of variation for R_s at large ΔS is similar in magnitude with the one obtained on stable nuclei from a consistent analysis of a large set of transfer reaction data but also from $(e,e'p)$ reactions (see Ref. [30], Figs. 1 and 2) in which most values were shown to scatter between 0.4 and 0.7 with a mean value of 0.55. It illustrates the maximum degree of precision currently within reach with such methods.

The most important influence on the C^2S_{exp} (and thus R_s) values is the choice of OFs. The study presented here demonstrates that it is important to have some means of applying a physical constraint on the range of acceptable r_0 values if using conventional WS based OFs since the unconsidered use of the popular choice of $r_0 = 1.25$ fm can have a significant impact on the results. Via a notch test we also demonstrated that for these particular systems the direct use of OFs calculated by an *ab initio* nuclear structure theory in the reaction calculations was meaningful since the angular distributions were sensitive to the OFs in a radial region where their fall-off remained physically reasonable and was not significantly affected by the practical constraints of the *ab initio* calculations. This radial sensitivity is of course specific to our study cases and must be checked individually in other conditions.

In conclusion, this study shows the value of evaluating the influence of different inputs to reaction calculations in analyses of this kind. Even if it is not possible to perform a sufficiently large number of calculations to yield statistically rigorous uncertainties on the extracted structure information useful information may still be obtained in this direction.

ACKNOWLEDGMENTS

The authors express their gratitude to Carlo Barbieri for helpful suggestions and a careful reading of the manuscript. This work was supported by the Polish National Science Centre under Contract No. 2013/08/M/ST2/00257 (LEA-COPIGAL) and POLONIUM PHC under Grant No. 22470XA.

[1] S. T. Butler, Phys. Rev. **80**, 1095 (1950).
[2] H. B. Burrows, W. H. Gibson, and J. Rotblat, Phys. Rev. **80**, 1095 (1950).
[3] J. R. Holt and C. T. Young, Proc. Phys. Soc. A **63**, 833 (1950).
[4] H. A. Bethe and S. T. Butler, Phys. Rev. **85**, 1045 (1952).
[5] M. H. Macfarlane and J. B. French, Rev. Mod. Phys. **32**, 567 (1960).
[6] A. Navin, D. W. Anthony, T. Aumann, T. Baumann, D. Bazin, Y. Blumenfeld, B. A. Brown, T. Glasmacher, P. G. Hansen, R. W. Ibbotson, P. A. Lofy, V. Maddalena, K. Miller, T. Nakamura, B. V. Pritychenko, B. M. Sherrill, E. Spears, M. Steiner, J. A. Tostevin, J. Yurkon, and A. Wagner, Phys. Rev. Lett. **85**, 266 (2000).
[7] J. P. Schiffer, S. J. Freeman, J. A. Caggiano, C. Deibel, A. Heinz, C. L. Jiang, R. Lewis, A. Parikh, P. D. Parker, K. E. Rehm, S. Sinha, and J. S. Thomas, Phys. Rev. Lett. **92**, 162501 (2004).
[8] A. Obertelli *et al.*, Phys. Lett. B **633**, 33 (2006).
[9] D. Suzuki, H. Iwasaki, D. Beaumel, L. Nalpas, E. Pollacco, M. Assie, H. Baba, Y. Blumenfeld, N. DeSereville, A. Drouart, S. Franchoo, A. Gillibert, J. Guillot, F. Hammache, N. Keeley, V. Lapoux, F. Marechal, S. Michimasa, X. Mougeot, I. Mukha, H. Okamura, H. Otsu, A. Ramus, P. Roussel-Chomaz, H. Sakurai, J. A. Scarpaci, O. Sorlin, I. Stefan, and M. Takechi, Phys. Rev. Lett. **103**, 152503 (2009).
[10] G. Burgunder, O. Sorlin, F. Nowacki, S. Giron, F. Hammache, M. Moukaddam, N. deSereville, D. Beaumel, L. Caceres, E. Clement, G. Duchene, J. P. Ebran, B. Fernandez-Dominguez, F. Flavigny, S. Franchoo, J. Gibelin, A. Gillibert, S. Grevy, J. Guillot, A. Lepailleur, I. Matea, A. Matta, L. Nalpas, A. Obertelli, T. Otsuka, J. Pancin, A. Poves, R. Raabe, J. A. Scarpaci, I. Stefan, C. Stodel, T. Suzuki, and J. C. Thomas, Phys. Rev. Lett. **112**, 042502 (2014).
[11] F. Raimondi, G. Hupin, P. Navrátil, and S. Quaglioni, Phys. Rev. C **93**, 054606 (2016).
[12] Y. Jaganathen, N. Michel, and M. Ploszajczak, Phys. Rev. C **89**, 034624 (2014).
[13] A. Kumar, R. Kanungo, A. Calci, P. Navratil, A. Sanetullaev, M. Alcorta, V. Bildstein, G. Christian, B. Davids, J. Dohet-Eraly, J. Fallis, A. T. Gallant, G. Hackman, B. Hadinia, G. Hupin, S. Ishimoto, R. Krucken, A. T. Laffoley, J. Lighthall, D. Miller, S. Quaglioni, J. S. Randhawa, E. T. Rand, A. Rojas, R. Roth, A. Shotter, J. Tanaka, I. Tanihata, and C. Unsworth, Phys. Rev. Lett **118**, 262502 (2017).
[14] G. J. Kramer *et al.*, Nucl. Phys. A **679**, 267 (2001).
[15] B. A. Brown, P. G. Hansen, B. M. Sherrill, and J. A. Tostevin, Phys. Rev. C **65**, 061601 (2002).
[16] G. R. Satchler, *Direct Nuclear Reactions* (Clarendon Press, Oxford, 1983).
[17] A. E. Lovell, F. M. Nunes, J. Sarich, and S. M. Wild, Phys. Rev. C **95**, 024611 (2017).
[18] F. Bjorklund, I. Blanford, and S. Fernbach, Phys. Rev. **108**, 795 (1957).
[19] F. Bjorklund and S. Fernbach, Phys. Rev. **109**, 1295 (1958).
[20] F. G. Perey, Phys. Rev. **131**, 745 (1963).
[21] A. E. Lovell and F. M. Nunes, J. Phys. G: Nucl. Part. Phys. **42**, 034014 (2015).
[22] A. Gade, D. Bazin, B. A. Brown, C. M. Campbell, J. A. Church, D. C. Dinca, J. Enders, T. Glasmacher, P. G. Hansen, Z. Hu, K. W. Kemper, W. F. Mueller, H. Olliver, B. C. Perry, L. A. Riley, B. T. Roeder, B. M. Sherrill, J. R. Terry, J. A. Tostevin, and K. L. Yurkewicz, Phys. Rev. Lett. **93**, 042501 (2004).
[23] A. Gade, P. Adrich, D. Bazin, M. D. Bowen, B. A. Brown, C. M. Campbell, J. M. Cook, T. Glasmacher, P. G. Hansen, K. Hosier, S. McDaniel, D. McGlinchery, A. Obertelli, K. Siwek, L. A. Riley, J. A. Tostevin, and D. Weisshaar, Phys. Rev. C **77**, 044306 (2008).
[24] J. A. Tostevin and A. Gade, Phys. Rev. C **90**, 057602 (2014).

[25] C. Louchart, A. Obertelli, A. Boudard, and F. Flavigny, Phys. Rev. C **83**, 011601(R) (2011).
[26] F. Flavigny, A. Obertelli, A. Bonaccorso, G. F. Grinyer, C. Louchart, L. Nalpas, and A. Signoracci, Phys. Rev. Lett. **108**, 252501 (2012).
[27] J. Lee, M. B. Tsang, D. Bazin, D. Coupland, V. Henzl, D. Henzlova, M. Kilburn, W. G. Lynch, A. M. Rogers, A. Sanetullaev, A. Signoracci, Z. Y. Sun, M. Youngs, K. Y. Chae, R. J. Charity, H. K. Cheung, M. Famiano, S. Hudan, P. OMalley, W. A. Peters, K. Schmitt, D. Shapira, and L. G. Sobotka, Phys. Rev. Lett. **104**, 112701 (2010).
[28] J. Lee, M. B. Tsang, D. Bazin, D. Coupland, V. Henzl, D. Henzlova, M. Kilburn, W. G. Lynch, A. M. Rogers, A. Sanetullaev, Z. Y. Sun, M. Youngs, R. J. Charity, L. G. Sobotka, M. Famiano, S. Hudan, D. Shapira, P. OMalley, W. A. Peters, K. Y. Chae, and K. Schmitt, Phys. Rev. C **83**, 014606 (2011).
[29] F. M. Nunes, A. Deltuva, and J. Hong, Phys. Rev. C **83**, 034610 (2011).
[30] B. P. Kay, J. P. Schiffer, and S. J. Freeman, Phys. Rev. Lett **111**, 042502 (2013).
[31] F. Flavigny, A. Gillibert, L. Nalpas, A. Obertelli, N. Keeley, C. Barbieri, D. Beaumel, S. Boissinot, G. Burgunder, A. Cipollone, A. Corsi, J. Gibelin, S. Giron, J. Guillot, F. Hammache, V. Lapoux, A. Matta, E. C. Pollacco, R. Raabe, M. Rejmund, N. deSereville, A. Shrivastava, A. Signoracci, and Y. Utsuno, Phys. Rev. Lett. **110**, 122503 (2013).
[32] E. C. Pollacco *et al.*, Eur. Phys. J. A **25**, 287 (2005).
[33] S. Pullanhiotan *et al.*, Nucl. Instr. and Meth. A **593**, 343 (2008).
[34] S. Ottini-Hustache *et al.*, Nucl. Inst. and Meth. A **431**, 476 (1999).
[35] V. Bechtold *et al.*, Phys. Lett. B **72**, 169 (1977).
[36] M. Gaillard *et al.*, Nucl. Phys. A **119**, 161 (1968).
[37] D. Hartwig *et al.*, Z. Physik **246**, 418 (1971).
[38] I. J. Thompson, Comput. Phys. Rep. **7**, 167 (1988).
[39] G. H. Rawitscher, Phys. Rev. C **11**, 1152 (1974).
[40] N. Keeley, N. Alamanos, and V. Lapoux, Phys. Rev. C **69**, 064604 (2004).
[41] R. V. Reid, Jr., Ann. Phys. (N.Y.) **50**, 411 (1968).
[42] A. J. Koning and J. P. Delaroche, Nucl. Phys. A **713**, 231 (2003).
[43] F. D. Becchetti and G. W. Greenlees, Phys. Rev. **182**, 1190 (1969).
[44] R. L. Varner *et al.*, Phys. Rep. **201**, 57 (1991).
[45] B. A. Watson *et al.*, Phys. Rev. **182**, 977 (1969).
[46] F. Hinterberger, G. Mairle, U. Schmidt-Rohr, G. J. Wagner, and P. Turek, Nucl. Phys. A **111**, 265 (1968).
[47] F. D. Bechetti Jr. and G. W. Greenlees, in *Polarization Phenomena in Nuclear Reactions*, edited by H. H. Barschall and W. Haeberli (University of Wisconsin Press, Madison, 1971), p. 682.
[48] C. M. Perey and F. G. Perey, At. Dat. and Nucl. Dat. Tab. **17**, 1 (1976).
[49] D. Y. Pang, P. Roussel-Chomaz, H. Savajols, R. L. Varner, and R. Wolski, Phys. Rev. C **79**, 024615 (2009).
[50] D. Y. Pang, W. M. Dean, and A. M. Mukhamedzhanov, Phys. Rev. C **91**, 024611 (2015).
[51] K. M. Nollett and R. B. Wiringa, Phys. Rev. C **83**, 041001 (2011).
[52] M. Leuschner, J. R. Calarco, F. W. Hersman, E. Jans, G. J. Kramer, L. Lapikas, G. vanderSteenhoven, P. K. A. deWittHuberts, H. P. Blok, N. Kalantar-Nayestanaki, and J. Friedrich, Phys. Rev. C **49**, 955 (1994).
[53] E. Chabanat *et al.*, Nucl. Phys. A **635**, 231 (1998).
[54] A. Cipollone, C. Barbieri, and P. Navratil, Phys. Rev. Lett. **111**, 062501 (2013).
[55] A. Cipollone, C. Barbieri, and P. Navratil, Phys. Rev. C **92**, 014306 (2015).
[56] V. Lapoux, V. Soma, C. Barbieri, H. Hergert, J. D. Holt, and S. R. Stroberg, Phys. Rev. Lett. **117**, 052501 (2016).
[57] A. Ekstrom, G. R. Jansen, K. A. Wendt, G. Hagen, T. Papenbrock, B. D. Carlsson, C. Forssen, M. Hjorth-Jensen, P. Navratil, and W. Nazarewicz, Phys. Rev. C **91**, 051301 (2015).
[58] A. Idini, C. Barbieri, and P. Navratil, Acta Phys. Pol. B **48**, 273 (2017).
[59] J. G. Cramer and R. M. De Vries, Phys. Rev. C **22**, 91 (1980).
[60] A. M. Eiro and I. J. Thompson, Phys. Rev. C **59**, 2670 (1999).
[61] Brida *et al.*, Phys. Rev. C **84**, 024319 (2011).
[62] G. F. Grinyer, D. Bazin, A. Gade, J. A. Tostevin, P. Adrich, M. D. Bowen, B. A. Brown, C. M. Campbell, J. M. Cook, T. Glasmacher, S. McDaniel, A. Obertelli, K. Siwek, J. R. Terry, D. Weisshaar, and R. B. Wiringa, Phys. Rev. C **86**, 024315 (2012).
[63] L. Atar *et al.*, Phys. Rev. Lett. **120**, 052501 (2018).
[64] W. W. Daehnick, J. D. Childs, and Z. Vrcelj, Phys. Rev. C **21**, 2253 (1980).
[65] See Supplemental Material at http://link.aps.org/supplemental/10.1103/PhysRevC.97.034601 for the values of experimental spectroscopic factors (C^2S_{exp}) obtained for each CRC calculation with the various combinations of optical potentials and overlap functions.